Reconfigurable Intelligent Surfaces Enhanced Symbol Level Interference Exploitation Precoding

Junwen Yang, *Graduate Student Member, IEEE,* Ang Li, *Senior Member, IEEE,* Xuewen Liao, *Member, IEEE,* Christos Masouros, *Fellow, IEEE,* and A. Lee Swindlehurst, *Fellow, IEEE*

***Abstract*—Reconfigurable intelligent surfaces (RIS)-aided communications are expected to provide increased degrees of freedom and enhanced performance in future wireless communications systems. This improvement is due to the ability of the RIS to optimize the propagation environment. In this letter, we investigate RIS-enhanced symbol-level interference exploitation precoding, an advanced interference management technique that can fully utilize multi-user interference to enhance the desired signals. Specifically, we formulate the precoding and RIS reflection design problem to minimize the transmit power, subject to constraints on the constructive interference (CI) and the RIS reflection coefficients. To solve this multivariable nonconvex optimization problem, we propose an efficient algorithm based on the alternating direction method of multipliers (ADMM), which allows the problem to be split into several simpler subproblems. Simulation results demonstrate that the proposed RIS-enhanced symbol-level interference exploitation precoding requires significantly lower transmit power to achieve a prescribed signal-to-interference-plus-noise ratio (SINR) threshold compared to benchmark schemes. Moreover, the proposed efficient algorithm is shown to converge within a limited number of iterations.**

***Index Terms*—Reconfigurable intelligent surfaces (RIS), interference management, constructive interference, interference exploitation precoding, symbol-level precoding.**

I. Introduction

Manuscript received 28 November 2024; revised 9 March 2025; accepted 13 April 2025. The work of Ang Li was supported in part by the Science and Technology Program of Shaanxi Province under Grant 2024JC-JCQN-59, and in part by the open research fund of the National Mobile Communications Research Laboratory, Southeast University (No. 2024D01). The work of Xuewen Liao was supported in part by the National Key Research and Development Program of China under Grant 2021YFB2900501, in part by the Shaanxi Science and Technology Innovation Team under Grant 2023-CX-TD-03, and in part by the Science and Technology Program of Shaanxi Province under Grant 2021GXLH-Z-038. The work of A. Lee Swindlehurst was supported by the U.S. National Science Foundation under Grant CNS-2107182. *(Corresponding authors: Xuewen Liao; Ang Li.)*

J. Yang is with the School of Information and Communications Engineering, Faculty of Electronic and Information Engineering, Xi'an Jiaotong University, Xi'an, Shaanxi 710049, China (e-mail: jwyang@stu.xjtu.edu.cn).

A. Li is with the School of Information and Communications Engineering, Faculty of Electronic and Information Engineering, Xi'an Jiaotong University, Xi'an, Shaanxi 710049, China, and also with the National Mobile Communications Research Laboratory, Southeast University, Nanjing 210096, China (e-mail: ang.li.2020@xjtu.edu.cn).

X. Liao is with the Shaanxi Key Laboratory of Deep Space Exploration Intelligent Information Technology, School of Information and Communications Engineering, Xi'an Jiaotong University, Xi'an, Shaanxi 710049, China (e-mail: yeplos@mail.xjtu.edu.cn).

C. Masouros is with the Department of Electronic and Electrical Engineering, University College London, London WC1E 7JE, U.K. (e-mail: c.masouros@ucl.ac.uk).

A. L. Swindlehurst is with the Center for Pervasive Communications and Computing, University of California, Irvine, CA 92697, USA (e-mail: swindle@uci.edu).

WIRELESS communications continue to evolve towards high energy and spectral efficiency. As part of this evolution, reconfigurable intelligent surfaces (RIS) technology has emerged as a key component of the vision for the future [1]. Composed of a large number of passive reflecting elements, RIS are known for their ability to adjust the phase of the reflected signal to direct it in desired directions. This concept offers new degrees of freedom in manipulating the effective channel state information (CSI). Transmit precoding is a CSI-aided signal processing technique that shapes the modulated signal such that the received signal quality is enhanced and multi-user interference is controlled. Depending on whether the precoder is updated in each transmission block or symbol slot, precoding can be categorized as either block-level or symbol-level [2]. Conventional block-level precoding utilizes only CSI to design the precoder, leading to interference suppression. On the other hand, symbol-level interference exploitation precoding (SLP) leverages both CSI and information about the data symbols, thus achieving superior performance [3].

In coordination with transmit beamforming/precoding, the RIS design problem is referred to as passive beamforming [4], while conventional transmit signal design is termed active beamforming. In [4], beamforming using an active antenna array at the transmitter and passive beamforming at the RIS are jointly optimized to minimize the total transmit power, subject to signal-to-interference-plus-noise ratio (SINR) constraints. To solve this problem, the authors propose two efficient suboptimal algorithms for the multi-user setup. The work in [5] considers the phase shift design problem for a given transmit beamforming strategy, ensuring that the reflected signal combines constructively at each user, while minimizing the symbol error rate. Additionally, [6] investigates the employment of RIS in symbol-level precoding systems, and the resulting joint optimization problem is decomposed into separate symbol-level precoding and block-level reflecting design problems. In [7], the deployment of an RIS in a heterogeneous network is considered and a multi-objective optimization problem is formulated to jointly minimize the transmit power at both a macro and pico base station (BS).

Existing work like that above has not considered RIS-enhanced SLP for general multi-user multi-antenna systems. Moreover, the development of efficient algorithms for jointly optimizing the RIS reflection coefficients and the interference exploitation precoding remains an open problem in the literature.

In this letter, we consider RIS-enhanced power minimization

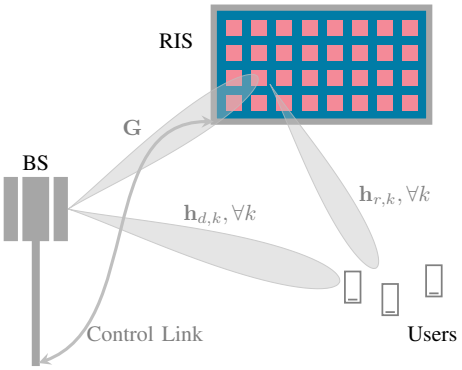

Fig. 1. An RIS-aided wireless communication system.

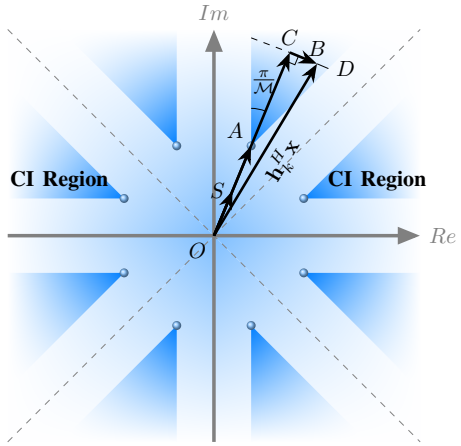

Fig. 2. Geometric interpretation of interference exploitation precoding for the 8PSK constellation, where $\mathcal{M} = 8$.

SLP. We design the multi-user interference to constructively contribute to the desired signal, ensuring that the received SINR of each user meets or exceeds a given threshold. The RIS reflection coefficients are constrained to be unit modulus, which makes the problem nonconvex. The presence of multiple variables and constraints in the optimization problem hinders finding the optimal solution. However, the structure of the problem naturally motivates us to split the variables and constraints and address them separately using more efficient algorithms for each subproblems. By adopting the alternating direction method of multipliers (ADMM), we introduce an auxiliary variable to split the reflection variables into two parts corresponds to the SINR and the unitary modulus constraints. The joint optimization problem is then decomposed into three subproblems, and we derive a closed-form solution to the unitary modulus constrained subproblem. Simulation results validate the effectiveness of the proposed algorithm.

II. System Model and Problem Formulation

We consider an RIS-aided multi-user multiple-input single-output (MISO) system, where a BS with N_t antennas simultaneously provides services for N_r single-antenna users, and an N_i-port RIS is deployed to aid the communication links. Additionally, the reflection coefficients of the RIS elements can be configured by the BS via a dedicated link. The channel for the direct link between the BS and user k is denoted as $\mathbf{h}_{d,k} \in \mathbb{C}^{N_t}$, the channel between the BS and RIS is denoted as $\mathbf{G} \in \mathbb{C}^{N_i \times N_t}$, and the reflection channel between the RIS and user k is denoted as $\mathbf{h}_{r,k} \in \mathbb{C}^{N_i}$, as shown in Fig. 1. We denote the modulated data symbol vector as $\mathbf{s} \triangleq [s_1, \cdots, s_{N_r}] \in \mathbb{C}^{N_r}$, and its associated precoder as $\mathbf{W}$. With both direct and reflected links, the received signal at user k can be modeled as

$$\begin{aligned} y_k =& \mathbf{h}_{d,k}^H \mathbf{W}\mathbf{s} + \mathbf{h}_{r,k}^H \mathbf{\Phi}\mathbf{G}\mathbf{W}\mathbf{s} + n_k \\ =& \mathbf{h}_k^H \mathbf{x} + n_k, \end{aligned} \tag{1}$$

where $\mathbf{\Phi} \in \mathbb{C}^{N_i \times N_i}$ denotes the reflection matrix of the RIS, and n_k represents additive white Gaussian noise with variance σ_k^2 at user k. The effective channel for user k is denoted as $\mathbf{h}_k^H \triangleq \mathbf{h}_{d,k}^H + \mathbf{h}_{r,k}^H \mathbf{\Phi}\mathbf{G}, \forall k$, and the combined channel for all users is given by

$$\mathbf{H} \triangleq \mathbf{H}_d + \mathbf{H}_r \mathbf{\Phi}\mathbf{G}, \tag{2}$$

where $\mathbf{H} \triangleq \left[\mathbf{h}_1, \cdots, \mathbf{h}_{N_r}\right]^H$, $\mathbf{H}_d \triangleq \left[\mathbf{h}_{d,1}, \cdots, \mathbf{h}_{d,N_r}\right]^H$, $\mathbf{H}_r \triangleq \left[\mathbf{h}_{r,1}, \cdots, \mathbf{h}_{r,N_r}\right]^H$.

In this letter, we directly optimize the transmitted signal $\mathbf{x} \triangleq \mathbf{W}\mathbf{s}$. We adopt a single connected RIS model, hence the signal impinging on a given RIS element is fully reflected by the same port, so the reflection matrix $\mathbf{\Phi}$ is diagonal. We assume the RIS is a passive device, so the reflected signal has the same power as the impinging signal. This property implies that the modulus of each diagonal element of $\mathbf{\Phi}$ is equal to 1. As a result, we have

$$\mathbf{\Phi} = \operatorname{diag}\left\{\boldsymbol{\phi}\right\}, \tag{3}$$

where $\boldsymbol{\phi} \triangleq [\phi_1, \cdots, \phi_{N_i}]^T$, $|\phi_i| = 1$. When there is attenuation in addition to reflection at the RIS, we have $|\phi_i| \leq 1$. In this case, the problem can be analyzed similarly. Therefore, we only consider the scenario without attenuation in this letter.

Interference exploitation precoding aims to design the transmit signal $\mathbf{x}$ given the effective channel and data symbol vector such that all the multi-user interference is constructive to the desired signal. To illustrate this concept, we take the 8 phase-shift keying (8PSK) constellation as an example. As shown in Fig. 2, we denote the data symbol of user k as $\overrightarrow{OS} = s_k$. When interference exploitation precoding is used, interference terms are eliminated from the instantaneous SINR of user k. The nominal constellation point associated with SINR threshold γ_k, where $\frac{\left|\mathbf{h}_k^H \mathbf{x}\right|^2}{\sigma_k^2} \geq \gamma_k \left|s_k\right|^2$, is given by $\overrightarrow{OA} = \sqrt{\gamma_k}\sigma_k s_k$. Using precoding, we hope to push the noiseless received signal $\overrightarrow{OB} = \mathbf{h}_k^H \mathbf{x}$ away from decision boundaries into the associated constructive interference (CI) region.

To model this design, we adopt the orthogonal decomposition proposed in [8]. First, we orthogonally decompose $\overrightarrow{OB}$ along the direction of the desired data symbol, as follows:

$$\overrightarrow{OB} = \overrightarrow{OC} + \overrightarrow{CB}. \tag{4}$$

Through this direct method, it follows directly that

$$\left|\overrightarrow{OC}\right| = \Re\left\{\frac{|s_k|}{s_k}\mathbf{h}_k^H \mathbf{x}\right\}, \left|\overrightarrow{CB}\right| = \left|\Im\left\{\frac{|s_k|}{s_k}\mathbf{h}_k^H \mathbf{x}\right\}\right|. \tag{5}$$

Denoting the intersection point of $\overrightarrow{CB}$ and the nearest CI region boundary as D, the geometric condition for $\overrightarrow{OB}$ to be located in the CI region can be explicitly written as

$$\left|\overrightarrow{CB}\right| - \left|\overrightarrow{CD}\right| \leq 0. \tag{6}$$

Keeping in mind that $\left|\overrightarrow{OA}\right| = \sqrt{\gamma_k}\sigma_k \left|s_k\right|$, we can convert the geometric condition in (6) into an algebraic condition using trigonometry, as shown below:

$$\left|\Im\left\{\frac{|s_k|}{s_k}\mathbf{h}_k^H\mathbf{x}\right\}\right| - \left(\Re\left\{\frac{|s_k|}{s_k}\mathbf{h}_k^H\mathbf{x}\right\} - \sqrt{\gamma_k}\sigma_k\left|s_k\right|\right) \times \tan\frac{\pi}{\mathcal{M}} \leq 0, \forall k. \tag{7}$$

As a step further, (7) can be equivalently rewritten as

$$\frac{1}{\tan\frac{\pi}{\mathcal{M}}}\left|\Im\left\{\frac{\mathbf{h}_k^H}{s_k}\mathbf{x}\right\}\right| - \Re\left\{\frac{\mathbf{h}_k^H}{s_k}\mathbf{x}\right\} + \sqrt{\gamma_k}\sigma_k \leq 0, \forall k. \tag{8}$$

It can be observed that the CI constraint in (8) not only guarantees that the noiseless received signal falls into its associated CI region, but also results in an SINR no smaller than the threshold γ_k. Given the modulus constraints on the RIS reflection coefficients and the SINR constraints in (8), we aim to design the transmit signal $\mathbf{x}$ and the diagonal elements of $\mathbf{\Phi}$ to minimize the transmit power, as follows:

$$\min_{\mathbf{x},\boldsymbol{\phi}} \|\mathbf{x}\|^2 \tag{9}$$

$$\text{s.t.}\frac{1}{\tan\frac{\pi}{\mathcal{M}}}\left|\Im\left\{\frac{\mathbf{h}_k^H}{s_k}\mathbf{x}\right\}\right| - \Re\left\{\frac{\mathbf{h}_k^H}{s_k}\mathbf{x}\right\} + \sqrt{\gamma_k}\sigma_k \leq 0, \forall k, \tag{10}$$

$$\mathbf{h}_k^H = \mathbf{h}_{d,k}^H + \mathbf{h}_{r,k}^H\mathbf{\Phi}\mathbf{G}, \forall k, \tag{11}$$

$$\mathbf{\Phi} = \text{diag}\left\{\boldsymbol{\phi}\right\}, |\phi_i| = 1, \forall i. \tag{12}$$

The joint symbol-level interference exploitation precoding and RIS configuration problem in (9) is a multivariable optimization problem with both convex and nonconvex constraints.

III. Efficient Algorithm

In this section, we address the RIS-enhanced SLP problem in (9) and propose an efficient iterative algorithm to solve it. The first obstacle arises from the absolute value operator in the SINR constraint. To address this, we split the original SINR constraint into two separate constraints, and we use the imaginary unit j to convert the imaginary operator into a real operator. The resultant SINR constraint is equivalently expressed as follows:

$$\frac{1}{\tan\frac{\pi}{\mathcal{M}}}\Re\left\{\frac{j\mathbf{h}_k^H}{s_k}\mathbf{x}\right\} - \Re\left\{\frac{\mathbf{h}_k^H}{s_k}\mathbf{x}\right\} + \sqrt{\gamma_k}\sigma_k \leq 0, \forall k, \tag{13}$$

$$\frac{-1}{\tan\frac{\pi}{\mathcal{M}}}\Re\left\{\frac{j\mathbf{h}_k^H}{s_k}\mathbf{x}\right\} - \Re\left\{\frac{\mathbf{h}_k^H}{s_k}\mathbf{x}\right\} + \sqrt{\gamma_k}\sigma_k \leq 0, \forall k. \tag{14}$$

The above derivations clarify that the SINR constraint is a system of linear inequalities in $\mathbf{x}$. Therefore, it is convex with respect to the transmit signal $\mathbf{x}$. Based on this transformation, the optimization problem can be written in a more tractable form as follows:

$$\min_{\mathbf{x},\boldsymbol{\phi}} \|\mathbf{x}\|^2 \tag{15}$$

$$\text{s.t.}\Re\left\{\mathbf{TS}\left(\mathbf{H}_d + \mathbf{H}_r\mathbf{\Phi}\mathbf{G}\right)\mathbf{x}\right\} + \mathbf{b} \leq 0, \tag{16}$$

$$\mathbf{\Phi} = \text{diag}\left\{\boldsymbol{\phi}\right\}, |\phi_i| = 1, \forall i. \tag{17}$$

where

$$\mathbf{T} \triangleq \begin{bmatrix}\left(\frac{j}{\tan\frac{\pi}{\mathcal{M}}} - 1\right)\mathbf{I} \\ \left(\frac{-j}{\tan\frac{\pi}{\mathcal{M}}} - 1\right)\mathbf{I}\end{bmatrix}, \mathbf{S} \triangleq \begin{bmatrix}\frac{1}{s_1} & & \\ & \ddots & \\ & & \frac{1}{s_{N_r}}\end{bmatrix}, \tag{18}$$

$$\mathbf{b} \triangleq \left[\sqrt{\gamma_1}\sigma_1, \cdots, \sqrt{\gamma_{N_r}}\sigma_{N_r}, \sqrt{\gamma_1}\sigma_1, \cdots, \sqrt{\gamma_{N_r}}\sigma_{N_r}\right]^T, \tag{19}$$

with $\mathbf{T} \in \mathbb{C}^{2N_r \times N_r}$, $\mathbf{S} \in \mathbb{C}^{N_r \times N_r}$, and $\mathbf{b} \in \mathbb{R}^{2N_r}$.

Although the SINR constraint has been transformed into a straightforward linear inequality constraint, the problem remains difficult to solve. Note that the SINR constraint involves two variables, each with a different feasible region. In particular, the feasible region for the transmit signal $\mathbf{x}$ is convex, while that for the reflection matrix $\mathbf{\Phi}$ is nonconvex. Moreover, the feasible region for $\mathbf{\Phi}$ is the intersection of two subspaces defined by the SINR and modulus constraints. We observe that the problem structure is well-suited for applying the splitting method, with one typical example being ADMM [9]. By taking advantage of this structure, we propose an efficient algorithm below for the reformulated RIS-enhanced SLP problem in (15).

Since the feasible region of $\boldsymbol{\phi}$ is jointly defined by the SINR and the modulus constraints, it is difficult to address them simultaneously. By introducing an auxiliary variable $\boldsymbol{\varphi}$ that is equal to $\boldsymbol{\phi}$, we can split the original variable $\boldsymbol{\phi}$ into two parts, each defined by a separate feasible region. The new problem is given by

$$\min_{\mathbf{x},\boldsymbol{\phi},\boldsymbol{\varphi}} \|\mathbf{x}\|^2 \tag{20}$$

$$\text{s.t.}\Re\left\{\mathbf{TSH}_d\mathbf{x} + \mathbf{TSH}_r\text{diag}\left\{\mathbf{G}\mathbf{x}\right\}\boldsymbol{\phi}\right\} + \mathbf{b} \leq 0, \tag{21}$$

$$|\varphi_i| = 1, \forall i, \tag{22}$$

$$\boldsymbol{\phi} = \boldsymbol{\varphi}. \tag{23}$$

To facilitate the following derivations, we denote the feasible regions defined by (21) and (22) as $\mathcal{C}$ and $\mathcal{D}$, respectively. The corresponding indicator functions are respectively defined as follows:

$$\mathbb{I}_{\mathcal{C}}\left(\mathbf{x}, \boldsymbol{\phi}\right) = \begin{cases}0, \text{if } \mathbf{x}, \boldsymbol{\phi} \in \mathcal{C}, \\ +\infty, \text{otherwise},\end{cases} \quad \mathbb{I}_{\mathcal{D}}\left(\boldsymbol{\varphi}\right) = \begin{cases}0, \text{if } \boldsymbol{\varphi} \in \mathcal{D}, \\ +\infty, \text{otherwise}.\end{cases} \tag{24}$$

Leveraging these definitions, problem (20) can be equivalently written as

$$\min_{\mathbf{x},\boldsymbol{\phi},\boldsymbol{\varphi}} \|\mathbf{x}\|^2 + \mathbb{I}_{\mathcal{C}}\left(\mathbf{x}, \boldsymbol{\phi}\right) + \mathbb{I}_{\mathcal{D}}\left(\boldsymbol{\varphi}\right) \tag{25}$$

$$\text{s.t.}\boldsymbol{\phi} = \boldsymbol{\varphi}. \tag{26}$$

In this way, RIS-enhanced SLP is transformed into an equality-constrained optimization problem, whose solution can be obtained with satisfactory convergence properties using ADMM [9].

The augmented Lagrangian function of (25) is given by

$$\mathcal{L}\left(\mathbf{x},\boldsymbol{\phi},\boldsymbol{\varphi},\boldsymbol{\nu}\right)=\left\|\mathbf{x}\right\|^{2}+\mathbb{I}_{\mathcal{C}}\left(\mathbf{x},\boldsymbol{\phi}\right)+\mathbb{I}_{\mathcal{D}}\left(\boldsymbol{\varphi}\right)+\Re\left\{\boldsymbol{\nu}^{H}\left(\boldsymbol{\phi}-\boldsymbol{\varphi}\right)\right\}+\frac{\rho}{2}\left\|\boldsymbol{\phi}-\boldsymbol{\varphi}\right\|^{2},\tag{27}$$

where ρ denotes the penalty parameter associated with the equality constraint in (26), and $\boldsymbol{\nu}$ is the corresponding Lagrange multiplier or dual variable. By minimizing the augmented Lagrangian function, the optimization variables can be alternatingly updated. In each iteration, the variables are updated as follows:

$$\left\{\mathbf{x}^{t+1},\boldsymbol{\phi}^{t+1}\right\}=\arg\min_{\{\mathbf{x},\boldsymbol{\phi}\}}\mathcal{L}\left(\mathbf{x},\boldsymbol{\phi},\boldsymbol{\varphi}^{t},\boldsymbol{\nu}^{t}\right),\tag{28}$$

$$\boldsymbol{\varphi}^{t+1}=\arg\min_{\boldsymbol{\varphi}}\mathcal{L}\left(\mathbf{x}^{t+1},\boldsymbol{\phi}^{t+1},\boldsymbol{\varphi},\boldsymbol{\nu}^{t}\right),\tag{29}$$

$$\boldsymbol{\nu}^{t+1}=\boldsymbol{\nu}^{t}+\rho\left(\boldsymbol{\phi}^{t+1}-\boldsymbol{\varphi}^{t+1}\right),\tag{30}$$

where t in the superscript denotes the iteration index. After convergence, we obtain the optimal solution to the RIS-enhanced SLP problem.

Inspecting the above iteration, we observe that the update for $\{\mathbf{x},\boldsymbol{\phi}\}$ is of high complexity due to the joint optimization of the two vectors. To reduce the complexity, we decompose the joint optimization problem for $\{\mathbf{x},\boldsymbol{\phi}\}$ into two simpler subproblems. In particular, we split the feasible region for $\mathcal{C}$ into two parts, $\mathcal{C}_1$ for $\mathbf{x}$ by fixing $\boldsymbol{\phi}$, and $\mathcal{C}_2$ for $\boldsymbol{\phi}$ obtained by fixing $\mathbf{x}$. Then the decomposed problems can be written as

$$\mathbf{x}^{t+1}=\arg\min_{\mathbf{x}}\left\|\mathbf{x}\right\|^{2}+\mathbb{I}_{\mathcal{C}_1}\left(\mathbf{x}\right),\tag{31}$$

$$\boldsymbol{\phi}^{t+1}=\arg\min_{\boldsymbol{\phi}}\mathbb{I}_{\mathcal{C}_2}\left(\boldsymbol{\phi}\right)+\Re\left\{\left\{\boldsymbol{\nu}^{t}\right\}^{H}\left(\boldsymbol{\phi}-\boldsymbol{\varphi}^{t}\right)\right\}+\frac{\rho}{2}\left\|\boldsymbol{\phi}-\boldsymbol{\varphi}^{t}\right\|^{2},\tag{32}$$

where $\mathcal{C}_1$ and $\mathcal{C}_2$ represent the feasible regions of $\mathbf{x}$ and $\boldsymbol{\phi}$, respectively. Note that while the splitting method provides satisfactory convergence behavior, it provides only an approximation of the optimal solution.

A. Update of $\mathbf{x}$

By explicitly stating the constraint represented by the indicator function in (31), the update of the transmit signal $\mathbf{x}$ can be formulated as the following optimization problem:

$$\min_{\mathbf{x}}\left\|\mathbf{x}\right\|^{2}\tag{33}$$

$$\text{s.t.}\Re\left\{\mathbf{TSH}_{d}\mathbf{x}+\mathbf{TSH}_{r}\text{diag}\left\{\boldsymbol{\phi}^{t}\right\}\mathbf{Gx}\right\}+\mathbf{b}\leq 0.\tag{34}$$

This is a linearly constrained quadratic programming problem, and moreover it is equivalent to conventional SLP without RIS. Since it is convex, its solution can be obtained using standard convex optimization tools.

B. Update of $\boldsymbol{\phi}$

For the update of the reflection vector $\boldsymbol{\phi}$ in (32), we rewrite the SINR constraint as a function of $\boldsymbol{\phi}$, resulting in the following formulation:

$$\min_{\boldsymbol{\phi}}\frac{\rho}{2}\left\|\boldsymbol{\phi}-\boldsymbol{\varphi}^{t}\right\|^{2}+\Re\left\{\left\{\boldsymbol{\nu}^{t}\right\}^{H}\left(\boldsymbol{\phi}-\boldsymbol{\varphi}^{t}\right)\right\},\tag{35}$$

$$\text{s.t.}\Re\left\{\mathbf{TSH}_{d}\mathbf{x}^{t+1}+\mathbf{TSH}_{r}\text{diag}\left\{\mathbf{Gx}^{t+1}\right\}\boldsymbol{\phi}\right\}+\mathbf{b}\leq 0.\tag{36}$$

The SINR constraints in (34) and (36) are linear constraints in $\mathbf{x}$ and $\boldsymbol{\phi}$, respectively, and their corresponding objective functions are both quadratic. Therefore, problem (35) is also convex and can be solved using standard solvers.

C. Update of $\boldsymbol{\varphi}$

We first substitute the augmented Lagrangian function (27) into (29) to obtain the following update for the auxiliary variable $\boldsymbol{\varphi}$:

$$\boldsymbol{\varphi}^{t+1}=\arg\min_{\boldsymbol{\varphi}}\mathbb{I}_{\mathcal{D}}\left(\boldsymbol{\varphi}\right)+\Re\left\{\left\{\boldsymbol{\nu}^{t}\right\}^{H}\left(\boldsymbol{\phi}^{t+1}-\boldsymbol{\varphi}\right)\right\}+\frac{\rho}{2}\left\|\boldsymbol{\phi}^{t+1}-\boldsymbol{\varphi}\right\|^{2}.\tag{37}$$

We then rewrite the indicator function in (37) as a regular constraint, obtaining the optimization problem for $\boldsymbol{\varphi}$ shown below:

$$\min_{\boldsymbol{\varphi}}\frac{\rho}{2}\left\|\boldsymbol{\phi}^{t+1}-\boldsymbol{\varphi}\right\|^{2}+\Re\left\{\left\{\boldsymbol{\nu}^{t}\right\}^{H}\left(\boldsymbol{\phi}^{t+1}-\boldsymbol{\varphi}\right)\right\},\tag{38}$$

$$\text{s.t.}\left|\varphi_{i}\right|=1,\forall i.\tag{39}$$

As indicated previously, the modulus constraint in (39) is nonconvex. Fortunately, problem (38) involves only one vector variable and a modulus constraint. A closed-form solution can be derived for problem (38) by aligning the phase of $\boldsymbol{\varphi}$ with the phase of $\boldsymbol{\phi}^{t+1}+\frac{1}{\rho}\boldsymbol{\nu}^{t}$.

Lemma 1: The optimal solution to problem (38) is given by

$$\boldsymbol{\varphi}^{t+1}=\exp\left\{j\angle\left(\boldsymbol{\phi}^{t+1}+\frac{1}{\rho}\boldsymbol{\nu}^{t}\right)\right\}.\tag{40}$$

To sum up, we have addressed all the subproblems in the proposed ADMM algorithm, which alternately updates the primal and dual variables to converge to a stationary point. The worst-case computational complexity of solving (33) and (35) using the interior-point method is $\mathcal{O}\left(N_t^3\right)$ and $\mathcal{O}\left(N_i^3\right)$, respectively. The computational complexity of (40) is $\mathcal{O}\left(N_i\right)$. Since we can obtain the optimal solution to each subproblem, the convergence performance of the proposed algorithm follows that of the standard ADMM.

IV. Simulation Results

We assume an N_t-antenna BS located at $(0,0,5)$ m, and N_r single-antenna users randomly located in a circular area centered at $(0,50,1)$ m with radius 3 m. An N_i-element RIS is positioned at $(0,55,1)$ m. We set $N_t=N_r=6$. Quadrature PSK (QPSK) is assumed in this section. The path loss model is $c_0 d_0^{-\alpha}$, where $c_0=-30$ dB, and d_0 and α denote the link distance in m and the path loss exponent, respectively. The path loss exponents of the BS-user, BS-RIS, and RIS-user links are set as 2, 2.4 and 2.8, respectively. Apart from large-scale fading, we also consider a Rician fading channel model with the Rician factor set to 3 dB to account for small-scale fading. The noise variance is set to $\sigma_k^2=-90$ dBm, $\forall k$. The proposed algorithm is initialized with $\phi_i^0=\varphi_i^0=e^{-j2\pi a_i}, a_i\sim\mathcal{U}(0,1),\forall i$, and $\boldsymbol{\nu}^0=0.5\times\mathbf{1}+0.5\times j\mathbf{1}$, where $\mathcal{U}$ denotes the uniform distribution.

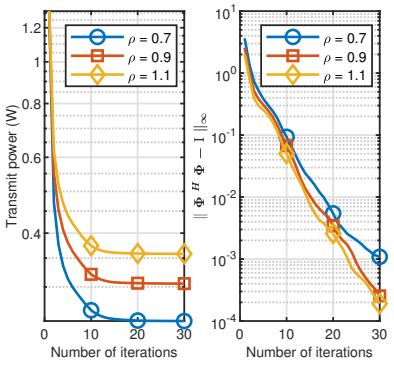

Fig. 3. Convergence of the proposed ADMM algorithm, $N_i = 32$, $\gamma_k = 24$ dB.

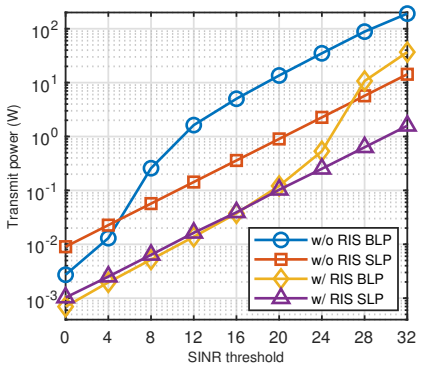

Fig. 4. The impact of SINR threshold on the total transmit power, $N_i = 32$.

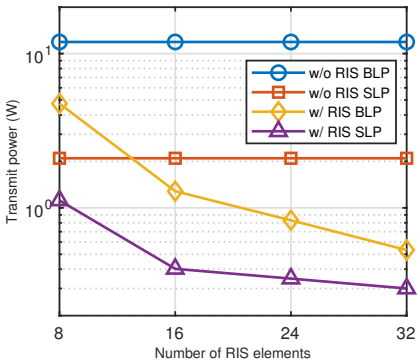

Fig. 5. The impact of number of RIS elements on the total transmit power, $\gamma_k = 24$ dB.

In Fig. 3, we illustrate the convergence performance of the proposed algorithm in terms of total transmit power and $\left\|\mathbf{\Phi}^H\mathbf{\Phi} - \mathbf{I}\right\|_\infty$ as a function of the number of iterations, where $N_i = 32$, and $\gamma_k = 24$ dB, $\forall k$. The different colored curves correspond to different choices of the penalty parameter ρ. The left figure shows that the transmit power is a monotonically non-increasing function of the number of iterations, taking about 10 iterations to converge to a stationary point. The right figure demonstrates the convergence behavior of the reflection matrix in terms of the degree to which it violates the unitary modulus constraint. The results show that the constraint is satisfied very accurately after 10-20 iterations. The rate of convergence is relatively unaffected by ρ, although reduced transmit power can be achieved for smaller values of ρ. In the remainder of the examples, we set the penalty parameter to $\rho = 0.7$, unless otherwise specified.

In Fig. 4, we analyze the impact of the SINR threshold on total transmit power, where $N_i = 32$. Optimal block-level precoding (BLP) with and without RIS, as proposed in [4] and [10], and optimal SLP [3] without RIS are selected as three benchmarks for comparison. The RIS-enhanced SLP solution is obtained using the proposed single-loop algorithm. The results indicate that RIS-enhanced SLP consumes the least transmit power to achieve the given SINR thresholds in medium to high SINR threshold regions, making it the most power-efficient approach. Additionally, the proposed algorithm is effective for a large range of SINR thresholds. The RIS-enhanced SLP approach outperforms its BLP counterpart in medium to high SINR threshold regions because the performance of BLP will severely deteriorate in such interference-limited scenarios.

In Fig. 5, we plot the total transmit power as a function of the number of RIS elements, where $\gamma_k = 24$ dB, $\forall k$, and $\rho = 4$ for $N_i = 8$. For the RIS-enhanced approaches, the total transmit power decreases with increasing N_i. It is natural that a larger RIS offers greater degrees of freedom to manipulate the channel, and an optimized channel requires less transmit power to achieve the SINR threshold. The proposed algorithm can effectively handle various scenarios involving different numbers of RIS elements.

V. Conclusion

This study considers RIS-enhanced symbol-level interference exploitation precoding. We jointly optimize the symbol-level interference exploitation precoding and the RIS reflection coefficients to minimize the total transmit power under both CI constraints and nonconvex constraints on the RIS coefficients. An efficient algorithm based on the ADMM framework is proposed to address the joint optimization problem, which splits the general problem into three subproblems. By alternately updating the solutions to the subproblems, followed by updating the dual variable, the algorithm can converge to a high quality solution. Various simulation results are provided to illustrate the effectiveness of the proposed algorithm.

References

[1] E. Basar *et al.*, "Reconfigurable intelligent surfaces for 6G: Emerging hardware architectures, applications, and open challenges," *IEEE Veh. Technol. Mag.*, vol. 19, no. 3, pp. 27–47, Sep. 2024.

[2] M. Alodeh *et al.*, "Symbol-level and multicast precoding for multiuser multiantenna downlink: A state-of-the-art, classification, and challenges," *IEEE Commun. Surveys Tuts.*, vol. 20, no. 3, pp. 1733–1757, 3rd Quart. 2018.

[3] A. Li *et al.*, "A tutorial on interference exploitation via symbol-level precoding: Overview, state-of-the-art and future directions," *IEEE Commun. Surveys Tuts.*, vol. 22, no. 2, pp. 796–839, 2nd Quart. 2020.

[4] Q. Wu and R. Zhang, "Intelligent reflecting surface enhanced wireless network via joint active and passive beamforming," *IEEE Trans. Wireless Commun.*, vol. 18, no. 11, pp. 5394–5409, Nov. 2019.

[5] A. Li, L. Song, B. Vucetic, and Y. Li, "Interference exploitation precoding for reconfigurable intelligent surface aided multi-user communications with direct links," *IEEE Wireless Commun. Lett.*, vol. 9, no. 11, pp. 1937–1941, Nov. 2020.

[6] R. Liu, M. Li, Q. Liu, and A. L. Swindlehurst, "Joint symbol-level precoding and reflecting designs for IRS-enhanced MU-MISO systems," *IEEE Trans. Wireless Commun.*, vol. 20, no. 2, pp. 798–811, Feb. 2021.

[7] H. Pang, F. Ji, M. Wen, S. Wang, L. Xu, and Y.-C. Wu, "Interference exploitation in IRS-aided heterogeneous networks: Joint symbol level precoding and reflecting design," *IEEE Trans. Wireless Commun.*, vol. 23, no. 6, pp. 6467–6481, Jun. 2024.

[8] J. Yang, A. Li, X. Liao, and C. Masouros, "Speeding-up symbol-level precoding using separable and dual optimizations," *IEEE Trans. Commun.*, vol. 71, no. 12, pp. 7056–7071, Dec. 2023.

[9] S. Boyd, N. Parikh, E. Chu, B. Peleato, and J. Eckstein, "Distributed optimization and statistical learning via the alternating direction method of multipliers," *Found. Trends Mach. Learn.*, vol. 3, no. 1, pp. 1–122, May 2011.

[10] A. Wiesel, Y. Eldar, and S. Shamai, "Linear precoding via conic optimization for fixed MIMO receivers," *IEEE Trans. Signal Process.*, vol. 54, no. 1, pp. 161–176, Jan. 2006.